The Journal of Chemical Physics

Interpreting the chemical mechanism in SERS using a Raman bond model

Cite as: J. Chem. Phys. **152**, 024126 (2020); https://doi.org/10.1063/1.5138204
Submitted: 13 November 2019 . Accepted: 26 December 2019 . Published Online: 14 January 2020

Ran Chen, and Lasse Jensen

COLLECTIONS

Paper published as part of the special topic on Emerging Directions in Plasmonics
Note: This paper is part of the JCP Special Topic on Emerging Directions in Plasmonics.

This paper was selected as an Editor's Pick

View Online Export Citation CrossMark

ARTICLES YOU MAY BE INTERESTED IN

Compressed intramolecular dispersion interactions
The Journal of Chemical Physics **152**, 024112 (2020); https://doi.org/10.1063/1.5126716

Numerical assessment for accuracy and GPU acceleration of TD-DMRG time evolution schemes
The Journal of Chemical Physics **152**, 024127 (2020); https://doi.org/10.1063/1.5135363

Analytical classical density functionals from an equation learning network
The Journal of Chemical Physics **152**, 021102 (2020); https://doi.org/10.1063/1.5135919

© 2020 Author(s).

AIP Publishing

The Journal of Chemical Physics ARTICLE scitation.org/journal/jcp

Interpreting the chemical mechanism in SERS using a Raman bond model

Cite as: J. Chem. Phys. 152, 024126 (2020); doi: 10.1063/1.5138204
Submitted: 13 November 2019 • Accepted: 26 December 2019 •
Published Online: 14 January 2020

View Online Export Citation CrossMark

Ran Chen and Lasse Jensen[a]

AFFILIATIONS

Department of Chemistry, Pennsylvania State University, University Park, Pennsylvania 16802, USA

Note: This paper is part of the JCP Special Topic on Emerging Directions in Plasmonics.
[a]**Electronic mail:** jensen@chem.psu.edu

ABSTRACT

We present a first-principles model that partitions Raman intensities to atomic and bond contributions. This framework allows us to interpret the chemical mechanism in surface-enhanced Raman scattering (SERS) as interatom charge flow modulations, which we define as Raman bonds. Hirshfeld partitioning and charge density localization are applied to express polarizability derivatives as charge flow modulations. Model systems consisting of pyridines, thiols, and carbenes interacting with metal clusters are studied using time-dependent density functional theory. We demonstrate that the mode-specific enhancements can be explained as Raman bonds conjugated across the molecule-metal interface. We also illustrate that the changes in Raman intensities induced by electric fields or chemical substitutions can generally be interpreted as changes of charge flows. The model is shown to work consistently for different types of molecule-metal bonds. Furthermore, our work shows that increasing the Raman bond conjugation across the interface leads to stronger chemical enhancements. The Raman bond model developed in this work provides a quantitative and intuitive interpretation of the chemical mechanism in SERS.

Published under license by AIP Publishing. https://doi.org/10.1063/1.5138204

I. INTRODUCTION

Surface-enhanced Raman scattering (SERS) has been widely applied as a single-molecule technique in chemical and biological detection.[1,2] Most of the enhancements can be attributed to the amplified local fields arising from the surface plasmon.[3,4] Distinguished from other single-molecule techniques, SERS provides vibrational fingerprint information from spectral signatures. This advantage enables SERS to monitor chemical reactions[5,6] or determine molecular adsorption conformations.[7] The vibrational fingerprint information has been directly visualized in high resolution images using tip-enhanced Raman scattering (TERS),[8] which combines SERS with scanning probe techniques.[9–11] The spectral signatures of SERS are mainly determined by the chemical interactions between molecules and surfaces.[12] Therefore, to extract the vibrational information, correct interpretations of the chemical mechanism in SERS are required.

The chemical mechanism is usually studied by modeling molecules interacting with metal clusters[13,14] or periodic slabs[15] using electronic structure methods. The interpretations are usually based on electronic structures. However, these interpretations are restrained to certain resonance conditions or types of molecule-metal bonds and offer semiquantitative analyses. Molecular resonance and charge transfer resonance have been proposed to contribute to the chemical enhancements by coupling to the surface plasmon.[14,16] The chemical mechanism is interpreted as vibrational modulations on the excitation energy and the transition dipole of the resonance. The enhancement specificity of vibrational modes can be explained as different modulations on molecular orbitals due to atomic motions.[15,17] However, it is difficult to quantify the orbital changes. The mode-specific enhancements have also been explained based on the symmetry of electronic and vibrational transitions,[18] but this interpretation presumes molecular surface configurations and only works for weakly bonded systems. At off resonance conditions, a large number of transitions are expected to contribute to the chemical enhancements. The chemical enhancements can be approximately explained by only comparing the excitation energies of the low-lying charge transfer states with the

molecular HOMO-LUMO gaps.[19–22] However, a quantitative interpretation of the mode specific enhancements is still missing. To quantitatively describe the chemical mechanism in SERS, case-by-case studies using electronic structure methods are required because the chemical enhancements are system and mode dependent. Therefore, a general and intuitive framework is desired for interpreting simulation results.

In this work, a framework called Raman bond model (RBM) is presented to interpret the chemical mechanism in SERS. Raman bonds are defined as charge flow modulations between atoms. Contributions to Raman intensities are assigned to individual bonds and directly correlated with vibrational modes. We find in general that the mode-specific enhancements can be interpreted as Raman bonds conjugated across the molecule-metal interface and increasing this conjugation leads to stronger chemical enhancements.

II. THEORY

An element of the polarizability tensor α_{ab} can be written as

$$\alpha_{ab} = -\int \boldsymbol{r}_b \delta\rho_a(\boldsymbol{r}) d\boldsymbol{r}, \tag{1}$$

where $-\boldsymbol{r}_b$ is the electronic dipole operator in direction b and $\delta\rho_a$ is the induced electron density caused by the external field in direction a. The induced density $\delta\rho_a$ can be partitioned to atomic contributions $\delta\rho_{i,a}$, which can be calculated as

$$\delta\rho_{i,a}(\boldsymbol{r}) = W_i \delta\rho_a(\boldsymbol{r}), \tag{2}$$

where W_i is the Hirshfeld partitioning weight[23] for atom i. α_{ab} can be rewritten as

$$\begin{aligned}\alpha_{ab} &= \sum_i \int -\boldsymbol{r}_b \delta\rho_{i,a}(\boldsymbol{r}) d\boldsymbol{r} \\ &= \sum_i \left\{ \int -(\boldsymbol{r}_b - \boldsymbol{R}_{i,b}) \delta\rho_{i,a}(\boldsymbol{r}) d\boldsymbol{r} - \boldsymbol{R}_{i,b} \int \delta\rho_{i,a}(\boldsymbol{r}) d\boldsymbol{r} \right\},\end{aligned} \tag{3}$$

where $\boldsymbol{R}_{i,b}$ is the nuclear coordinate for atom i in direction b. The first term on the right side describes the atomic contributions to the polarizability. The integral of the atomic induced density in the second term is the induced atomic charge $q_{i,a}$,

$$q_{i,a} = \int -\delta\rho_{i,a}(\boldsymbol{r}) d\boldsymbol{r}. \tag{4}$$

The value of the second term in Eq. (3) depends on the choices of origin. The origin dependence can be removed by allocating atomic induced charges to charge flows between atoms,

$$q_{i,a} = \sum_{j \neq i} q_{ij,a}, \tag{5}$$

where $q_{ij,a}$ is the charge flow between atom i and j caused by the external field in direction a. To obtain the charge flows, we adopt the Loprop method[24] where the objective function L is minimized using the method of Lagrange multipliers,

$$L = \sum_{ij} f(R_{ij}) q_{ij,a} + \sum_i \lambda_i \left(q_{i,a} - \sum_{j,j \neq i} q_{ij,a} \right), \tag{6}$$

where λ is the Lagrange multiplier applying the constraint that the atomic charges are not altered due to the allocation. $f(R_{ij})$ is a penalty function of the distance between atom i and j (R_{ij}) limiting long-range charge flows. The penalty function proposed in the Loprop method is

$$f(R_{ij}) = \exp\left\{ c \times \left(\frac{R_{ij}}{R_i^{\mathrm{cov}} + R_j^{\mathrm{cov}}} \right)^2 \right\}, \tag{7}$$

where R_i^{cov} is the covalent radius for atom i[25] and c is a coefficient tuning the penalty. To limit long-range charge flows, sufficient penalty is required. However, to reproduce the polarizability, excessive penalty needs to be avoided. In SERS studies, using one coefficient c is difficult to achieve this balance because the polarizabilities vary significantly from molecules to metal clusters. Therefore, in this work, the penalty function is modified,

$$f(R_{ij}) = \begin{cases} \exp\left\{ c \times \left(\frac{R_{ij}}{R_i^{\mathrm{cov}} + R_j^{\mathrm{cov}}} \right)^2 \right\} & \text{if } R_{ij} < 1.1(R_i^{\mathrm{cov}} + R_j^{\mathrm{cov}}) \\ \exp\left\{ 2c \times \left(\frac{R_{ij}}{R_i^{\mathrm{cov}} + R_j^{\mathrm{cov}}} \right)^2 \right\} & \text{if } R_{ij} \geq 1.1(R_i^{\mathrm{cov}} + R_j^{\mathrm{cov}}). \end{cases} \tag{8}$$

$c = 2$ is applied to all the systems studied in this work. Charge flows are limited to short ranges, and the polarizabilities are reproduced. This specific choice for the penalty function is discussed in detail in the supplementary material. The partitioning of the polarizability α_{ab} is then expressed as

$$\alpha_{ab} = \sum_i \left\{ -\int (\boldsymbol{r}_b - \boldsymbol{R}_{i,b}) \delta\rho_{i,a} d\boldsymbol{r} \right\} + \sum_{ij,j>i} \left\{ q_{ij,a} (\boldsymbol{R}_{i,b} - \boldsymbol{R}_{j,b}) \right\}, \tag{9}$$

which is now origin independent. Because Raman intensities are proportional to squared polarizability derivatives with respect to vibrational modes Q_k, the chemical mechanism in SERS can be interpreted by analyzing the polarizability derivative,

$$\frac{\partial \alpha_{ab}}{\partial Q_k} = \sum_i \frac{\partial \left\{ -\int (\boldsymbol{r}_b - \boldsymbol{R}_{i,b}) \delta\rho_{i,a} d\boldsymbol{r} \right\}}{\partial Q_k} + \sum_{ij,j>i} \frac{\partial \left\{ q_{ij,a} (\boldsymbol{R}_{i,b} - \boldsymbol{R}_{j,b}) \right\}}{\partial Q_k}. \tag{10}$$

The first term in the above equation describes the changes in the atomic induced charge densities, which is denoted as R^{atom}. The second term is defined as Raman bonds (R^{bond}). It describes the modulations of charge flows between atoms. We find that this term is the dominant contributions to Raman intensities, which we will discuss in detail later in this article.

III. COMPUTATIONAL DETAILS

All calculations in this work were performed using a local version of the Amsterdam density functional (ADF) program package.[26,27] The Becke-Perdew (BP86) XC-potential[28,29] and an all-electron triple-ζ polarized (TZP) slater type basis set from the ADF basis set library were used. The scalar relativistic effects were accounted for by the zeroth-order regular approximation (ZORA).[30] For the systems in this work, full geometry optimization and frequency calculations were performed. The vibrational frequencies and normal modes were calculated within the harmonic approximation. Polarizability calculations were performed using the AOResponse module[31,32] at zero frequency with the Adiabatic Local

Published under license by AIP Publishing

Density Approximation (ALDA). Polarizability derivatives were calculated by numerical differentiation with respect to the normal mode displacements. For any system in this work, the molecule-cluster axis is aligned with the x-axis and only the xx components in the polarizabilities are considered in the analyses. All the figures in this work are plotted using PyMOL.[33]

IV. RESULTS AND DISCUSSION

The study of the chemical mechanism starts by interpreting the difference between enhancements of vibrational modes. The spectra of $\partial\alpha_{xx}/\partial Q_k$ are plotted for a free pyridine (Py) and a pyridine on a Ag_{20} cluster (Py–Ag_{20}) in Fig. 1(a). The enhancements of a ring breathing mode ν_1 (976.07 cm^{-1} in Py and 996.17 cm^{-1} in Py–Ag_{20}) and a symmetric ring deformation mode ν_{12} (1019.80 cm^{-1} in Py and 1025.30 cm^{-1} in Py–Ag_{20}) are interpreted using the RBM.

In Py, modes ν_1 and ν_{12} both belong to A_1 symmetry in the C_{2v} point group and have similar Raman intensities. R^{atom} and R^{bond} are plotted in Fig. 1(b) and represented as spheres and cylinders, respectively. The geometric volumes of the spheres and cylinders characterize the magnitudes of R^{atom} and R^{bond}. The details of the calculations are provided in the supplementary material. For both modes, the Raman bonds corresponding to the aromatic bonds are the main contributions to the Raman intensities. The reason is that the aromatic bonds provide major charge flows. The constructive Raman bonds are labeled red and the destructive Raman bonds are labeled blue, meaning that charge flows in different bonds are modulated with different phases. The distributions of constructive and destructive Raman bonds change from mode ν_1 to ν_{12}, indicating that the phases of bond deformation determine the phases of charge flow modulations. The interference between Raman bonds provides two general causes for weak Raman intensities: One is that the vibrations do not modulate charge flows effectively, expressed as weak Raman bonds, and the other is that the charge flow modulations cancel each other, expressed as symmetrically distributed constructive and destructive Raman bonds.

In Py–Ag_{20}, mode ν_1 is more enhanced than ν_{12} because mode ν_1 has stronger Raman bonds and fewer destructive Raman bonds than ν_{12}, which is shown in Fig. 1(c). The different enhancements result from different N–Ag Raman bonds. A more effective modulation on the charge flow in the N–Ag bond is exerted by mode ν_1 than ν_{12} because of the larger N–Ag stretching at mode ν_1. This is reflected as a stronger N–Ag Raman bond at mode ν_1. Because the π backbonding between Py and Ag_{20}[19] connects the delocalized electrons in the fragments, the Raman bonds in the aromatic ring and Ag_{20} are conjugated via the N–Ag Raman bond. Here, we analogize the conjugation idea for chemical bonds to Raman bonds. The stronger N–Ag Raman bond at mode ν_1 leads to a stronger Raman bond conjugation across the molecule-metal interface, which causes stronger Raman bonds and turns the destructive Raman bonds in the free pyridine to constructive. In contrast, the weaker N–Ag Raman bond at mode ν_{12} leads to a weaker Raman bond conjugation across the interface, which causes weaker Raman bonds and preserves the original Raman bond pattern in the free pyridine.

The RBM is also applied to interpret the influence of the interaction between Py and Ag_{20} on the Raman intensities. Electric fields are widely applied to tune the molecule-metal interaction, and their effect on SERS enhancements has been studied theoretically at the Hartree-Fock level of theory.[34] Electric fields are applied to Py–Ag_{20}, and the spectra of α_{xx} derivatives for Py–Ag_{20} with different electric fields are shown in the supplementary material. Here, we focus on the changes in the Raman intensity at a C–H in plane bending mode. The frequency of the C–H in plane bending mode is 1200.90 cm^{-1} in Py–Ag_{20}, 1200.44 cm^{-1} in Py–Ag_{20} with the negative field, and 1203.67 cm^{-1} in Py–Ag_{20} with the positive field. The changes in its Raman intensity are interpreted using the RBM in Fig. 2. The Raman intensity is enhanced by the negative field and reduced by the positive field, reflected as stronger Raman bonds in Fig. 2(a) and weaker Raman bonds in Fig. 2(c). Because a common mode is compared, the Raman bond difference can be attributed to the charge flow changes caused by the applied fields. The negative field increases the interfragment charge flow, which increases the Raman bond conjugation across the molecule-metal interface and leads to stronger Raman bonds. In contrast, the positive field decreases the

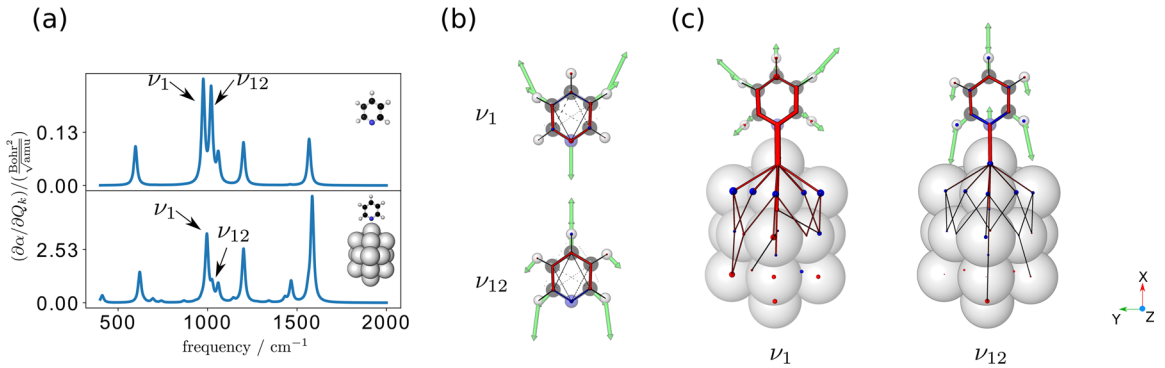

FIG. 1. The spectra of the α_{xx} derivatives with respect to vibrational modes from 400 cm^{-1}–2000 cm^{-1} are plotted in (a) for Py (the upper panel) and Py–Ag_{20} (the lower panel). R^{atom} and R^{bond} of the modes labeled in (a) are plotted for Py in (b) and for Py–Ag_{20} in (c). The green vectors are the vibrational mode vectors. The coordinate axes are demonstrated at the right side.

Published under license by AIP Publishing

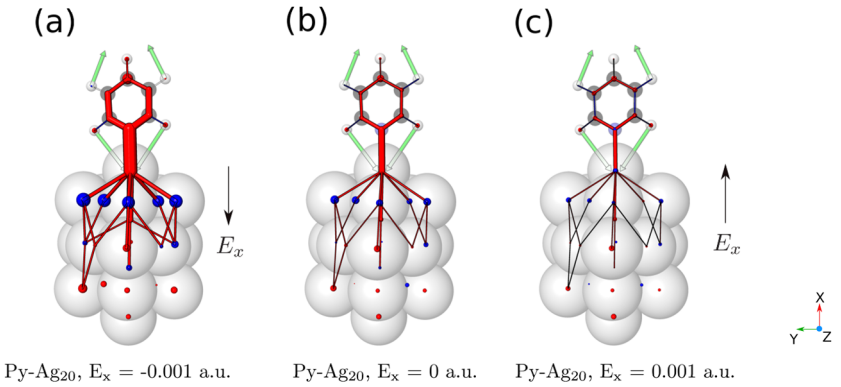

FIG. 2. The electric fields are applied along with the *x* axis and the positive direction is from the cluster to the molecule. R^{atom} and R^{bond} are plotted for Py–Ag_{20} at a C–H in plane bending mode (a) with a negative electric field, (b) with no field, and (c) with a positive electric field.

charge flows and the Raman bond conjugation which leads to weaker Raman bonds and destructive Raman bonds. The destructive Raman bonds recover the Raman bond pattern in the free pyridine, which means that the Raman bonds in the molecule are less affected by the Raman bonds in the cluster due to the decreased Raman bond conjugation.

To understand the effect of chemical substitutions on Raman intensities, chemical substitutions are applied to Py–Ag_{20} to tune the Raman intensity at the same C–H in plane bending mode. Py is substituted at the *para* site by a chlorine atom (PyCl–Ag_{20}) or an amino group ($PyNH_2$–Ag_{20}). The frequency of the C–H in plane bending mode is 1200.87 cm^{-1} in PyCl–Ag_{20} and 1202.86 cm^{-1} in $PyNH_2$–Ag_{20}. Corresponding R^{atom} and R^{bond} are plotted in Figs. 3(a) and 3(c). The chlorine substituent enhances the Raman intensity and the Raman bonds become stronger. The amino substituent reduces the Raman intensity, reflected as weaker Raman bonds and destructive Raman bonds. The destructive Raman bonds recover the Raman bond pattern in the free pyridine. The different Raman bond patterns also result from the changes of Raman bond conjugation. The chlorine substituent increases the conjugation, leading to stronger Raman bonds, and the amino substituent decreases the conjugation, leading to weaker Raman bonds and destructive Raman bonds. Considering that the Raman bonds are changed similarly by chemical substitutions or electric fields, we propose that chemical substitutions and electric fields are equivalent in tuning Raman intensities by changing charge flows. To further demonstrate the equivalence, a negative field is applied to $PyNH_2$–Ag_{20} at the same C–H in plane bending mode whose frequency is changed to 1204.67 cm^{-1}. R^{atom} and R^{bond} are plotted in Fig. 3(d). Because of the applied field, Raman bonds in general become stronger and destructive Raman bonds become constructive. The Raman bond changes caused by the amino substituent are reversed by the applied field, which supports that chemical substitutions and electric fields are equivalent in tuning Raman intensities by changing charge flows.

In summary, the negative field or the chlorine substituent increased the interfragment charge flow, while the positive field or the amino substituent decreased the interfragment charge flow. However, considering electron transfer from Py to Ag_{20} when Py is adsorbed on Ag_{20}, the negative field or the chlorine substituent was expected to pull electrons back to Py and decrease the interfragment charge flow. Similarly, the positive field or the amino

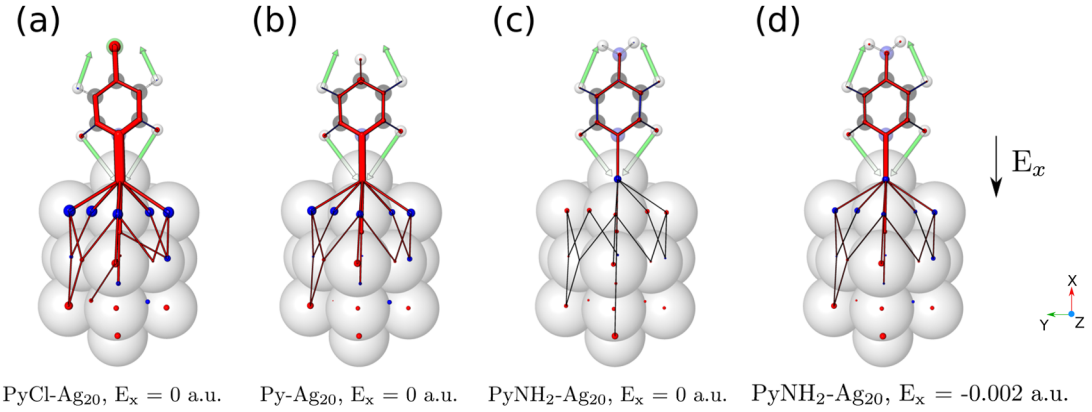

FIG. 3. R^{atom} and R^{bond} are plotted for (a) PyCl–Ag_{20}, (b) Py–Ag_{20}, (c) $PyNH_2$–Ag_{20}, and (d) $PyNH_2$–Ag_{20} under an applied field at the same C–H in plane bending mode studied in Fig. 2.

Published under license by AIP Publishing

substituent was expected to push electrons to Ag_{20} and increase the interfragment charge flow. To address this confusion, we consider the ground state charge transfer q^{GCT} defined as the sum of atomic charges in the molecule at the ground state. q^{GCT} is decreased by the negative field or the chlorine substituent, while increased by the positive field or the amino substituent, which is consistent with our expectation. The concept of "pushing or pulling electrons" refers to the electron behavior at the ground state. Although q^{GCT} and charge flows are intrinsically correlated, the derivation from one to the other is not trivial and their relation varies from system to system.

To study Raman bond patterns for different types of molecule-metal bonds, a propanethiol molecule on a Ag_{19} cluster (A–Ag_{19}) is studied. The structure is shown in Fig. 4(a). R^{atom} and R^{bond} at the S–Ag stretching mode (368.98 cm^{-1} in A–Ag_{19}) are plotted in Fig. 4(b). The S–Ag Raman bond is dominant, and no significant Raman bonds are generated in the fragments, indicating that the S–Ag Raman bond is not conjugated with other Raman bonds in the fragments. The reason is that S–Ag is a σ bond[19,35] and not conjugated with other bonds. To further demonstrate the lack of conjugation between the S–Ag Raman bond and other Raman bonds, a double bond is introduced to the C2–C3 (2E–Ag_{19}) or C1–C2 (1E–Ag_{19}) bond. R^{atom} and R^{bond} at their S–Ag stretching modes (330.57 cm^{-1} in 2E–Ag_{19} and 313.88 cm^{-1} in 1E–Ag_{19}) are shown in Fig. 4(b). Because the S–Ag σ bond cannot conjugate with the introduced double bond, the Raman bond pattern is not changed significantly, regardless of the position of the double bond.

Considering that the double bond has the capability of conjugating with the Ag–Ag bonds in the cluster, it is expected that stretching the double bond will cause conjugated Raman bonds. A stronger Raman bond conjugation is thus expected in 1E–Ag_{19} than in 2E–Ag_{19} as the double bond is closer to the cluster. R^{atom} and R^{bond} in 2E–Ag_{19} and 1E–Ag_{19} at their double bond stretching modes (1635.03 cm^{-1} in 2E–Ag_{19} and 1585.39 cm^{-1} in 1E–Ag_{19}) are shown in Fig. 4(c). The Raman bonds outside the thiol molecule in 1E–Ag_{19} are stronger at the double bond stretching mode than at the S–Ag stretching mode. This means that the vibrations establishing the Raman bond conjugation across the molecule-metal interface result in stronger Raman bonds from the cluster and have larger Raman intensities. The comparison of the Raman bonds between 2E–Ag_{19} and 1E–Ag_{19} at their double bond stretching modes shows that a larger Raman intensity can be obtained by increasing the Raman bond conjugation across the interface.

To further demonstrate the importance of the Raman bond conjugation to the chemical enhancements, the contributions to the Raman intensity from the molecule (R^{mol}), the interfragment bonds (R^{inter}), and the cluster ($R^{cluster}$) are compared between 2E–Ag_{19} and 1E–Ag_{19}. The contributions are averaged over the vibrations in the range from 300 cm^{-1}–2000 cm^{-1} because 2E–Ag_{19} and 1E–Ag_{19} have different vibrational modes. The ratio of the averaged contributions $\langle R^{mol}\rangle$:$\langle R^{inter}\rangle$:$\langle R^{cluster}\rangle$ is 0.31:0.32:0.37 in 2E–Ag_{19}. Normalized with respect to $\langle R^{mol}\rangle + \langle R^{inter}\rangle + \langle R^{cluster}\rangle$ of 2E–Ag_{19}, $\langle R^{mol}\rangle$:$\langle R^{inter}\rangle$:$\langle R^{cluster}\rangle$ in 1E–Ag_{19} is 0.29:0.78:0.96. This means that the averaged Raman intensity of 1E–Ag_{19} is 4.1 times as large as that of 2E–Ag_{19}. The main contributions to the larger Raman intensity in 1E–Ag_{19} are the S–Ag Raman bond and the Raman bonds in the cluster. The reason is that in 1E–Ag_{19}, any molecular vibration stretching the double bond will generate stronger Raman bonds outside the thiol molecule than 2E–Ag_{19} because of the increased Raman bond conjugation in 1E–Ag_{19}. This means that increasing the Raman bond conjugation across the molecule-metal interface leads to stronger chemical enhancements.

N-heterocyclic carbenes on gold surfaces are another group of SERS systems with strong chemical molecule-metal bonds. They are promising to provide better surface functionalizability than thiols because of their resilience under harsh chemical conditions.[36] To understand the Raman bond behavior in this bonding environment, a system consisting of a *N*-heterocyclic carbene on a Au_{20} cluster (Cb–Au_{20}) is studied using the RBM. The structure of Cb–Au_{20} is shown in Fig. 5(a), and the spectra of R^{mol}, R^{inter}, and $R^{cluster}$ are plotted in Fig. 5(b). The spectra show that R^{mol} are the dominant contributions to the significant Raman peaks, indicating that major Raman bonds are located in Cb. The reason is revealed by the structure of Cb–Au_{20} where the gold atom connected to Cb is pulled out from the surface. The isolation of Cb makes the

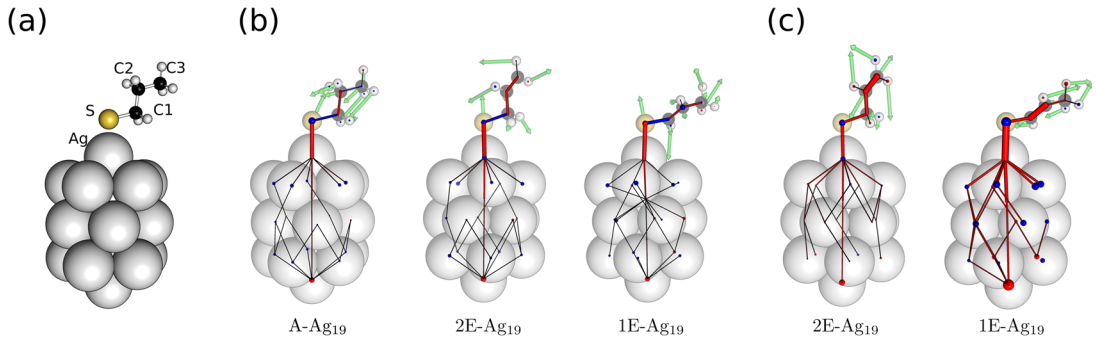

FIG. 4. The structure of A–Ag_{19} is shown in (a). The double bond can be introduced to C2–C3 (2E–Ag_{19}) or C1–C2 (1E–Ag_{19}). R^{atom} and R^{bond} in A–Ag_{19}, 2E–Ag_{19}, and 1EAg_{19} at the S–Ag stretching mode are plotted in (b). R^{atom} and R^{bond} in 2E–Ag_{19} and 1E–Ag_{19} at their double bond stretching modes are plotted in (c).

Published under license by AIP Publishing

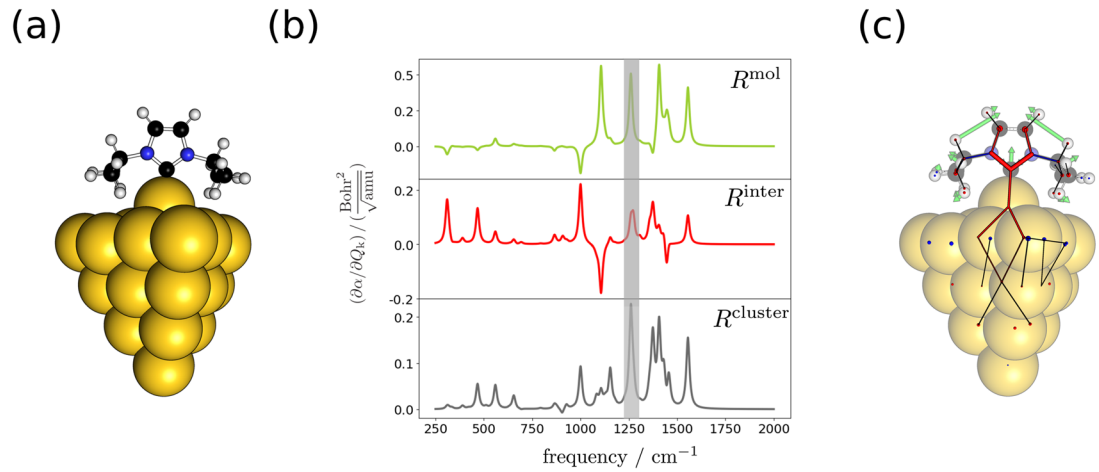

FIG. 5. The structure of Cb–Au_{20} is shown in (a). The spectra of R^{mol}, R^{inter}, and $R^{cluster}$ from 300 cm^{-1}–2000 cm^{-1} are plotted in (b). R^{atom} and R^{bond} at a mode highlighted in gray in the spectra are shown in (c).

Raman bonds in Cb not conjugated with the Raman bonds in Au_{20}, which leads to small $R^{cluster}$ and R^{inter}. Another spectral pattern is the interference between R^{inter} and R^{mol} or $R^{cluster}$, showing that the C–Au Raman bond is not conjugated with the Raman bonds in Cb or Au_{20}. The reason is that C–Au is a σ bond,[36] which is also responsible for the lack of the Raman bond conjugation. Time-dependent density functional theory (TDDFT) studies of carbenes on gold surfaces employing the Au_{20} cluster offered Raman spectra that agreed with experiments.[37] Because TDDFT tends to overestimate charge transfers between fragments, limited charge flow modulations between fragments are expected to alleviate the possible overestimation. This idea is supported by the small R^{inter} component in Fig. 5(b). Considering the small size of the Au_{20} cluster, the agreement also indicates that the charge flow modulations in the cluster are localized near the carbene. To represent the general Raman bond distribution in the cluster, R^{atom} and R^{bond} at the mode (1260.93 cm^{-1}) with the largest $R^{cluster}$ are plotted in Fig. 5(c). The weak and locally distributed Raman bonds in Au_{20} suggest that Au_{20} is sufficiently large to capture most charge flow modulations in the surface.

V. CONCLUSIONS

To obtain an intuitive and quantitative framework for interpreting the chemical mechanism in SERS, a Raman bond model was proposed in this work. Raman bonds are calculated from polarizability derivatives via Hirshfeld partitioning and charge density localization. Although, Hirshfeld partitioning was chosen for its basis independence and chemically intuitive results,[38,39] other atomic charge models based on charge densities are also compatible and the limitations of Hirshfeld partitioning can, in principle, be mitigated using the iterative Hirshfeld scheme.[40] Although charge flows are not uniquely determined given a set of atomic charges, a stable charge flow pattern can be achieved if long-range charge flows are limited and polarizabilities are reproduced. The applicability of this framework is shown for different types of molecule-metal bonds. We find that mode-specific enhancements can be interpreted as Raman bonds conjugated across the molecule-surface interface. The Raman bond conjugation can be established when molecular vibrations involve bonds conjugated with the bonds in clusters. Stronger chemical enhancements can be achieved by increasing the Raman bond conjugation, which can be induced by electric fields, chemical substitutions, and tuning molecular structures. The framework can also be potentially applied to quantify the effect of tunneling on TERS spectra[41] and interpret SERS or TERS observations of electrochemical reactions.[42] Facilitated by experimental Raman spectra, this framework can help us to understand charge transport in molecular electronic devices.[43]

SUPPLEMENTARY MATERIAL

See the supplementary material for the equations used to plot R^{atom} and R^{bond}. The spectra of α_{xx} derivatives with respect to vibrational modes for Py–Ag_{20} with different electric fields are shown. Tests on the penalty functions are discussed.

ACKNOWLEDGMENTS

The authors gratefully acknowledge financial support from National Science Foundation (Grant No. CHE-1707657). Simulations in this work were conducted in part with Advanced Cyber infrastructure computational resources provided by the Institute for Cyber-Science at the Pennsylvania State University (https://ics.psu.edu/).

REFERENCES

[1]K. A. Willets and R. P. Van Duyne, "Localized surface plasmon resonance spectroscopy and sensing," Ann. Rev. Phys. Chem. **58**, 267–297 (2007).
[2]P. L. Stiles, J. A. Dieringer, N. C. Shah, and R. P. Van Duyne, "Surface-enhanced Raman spectroscopy," Annu. Rev. Anal. Chem. **1**, 601–626 (2008).
[3]P. Johansson, H. Xu, and M. Käll, "Surface-enhanced Raman scattering and fluorescence near metal nanoparticles," Phys. Rev. B **72**, 035427 (2005).

Published under license by AIP Publishing

[4]S.-Y. Ding, E.-M. You, Z.-Q. Tian, and M. Moskovits, "Electromagnetic theories of surface-enhanced Raman spectroscopy," Chem. Soc. Rev. **46**, 4042–4076 (2017).
[5]E. Cortés, P. G. Etchegoin, E. C. Le Ru, A. Fainstein, M. E. Vela, and R. C. Salvarezza, "Monitoring the electrochemistry of single molecules by surface-enhanced Raman spectroscopy," J. Am. Chem. Soc. **132**, 18034–18037 (2010).
[6]Y. F. Huang, H. P. Zhu, G. K. Liu, D. Y. Wu, B. Ren, and Z. Q. Tian, "When the signal is not from the original molecule to be detected: Chemical transformation of *para*-aminothiophenol on Ag during the SERS measurement," J. Am. Chem. Soc. **132**, 9244–9246 (2010).
[7]C. Jing and Y. Fang, "Experimental (SERS) and theoretical (DFT) studies on the adsorption behaviors of L-cysteine on gold/silver nanoparticles," Chem. Phys. **332**, 27–32 (2007).
[8]J. Lee, K. T. Crampton, N. Tallarida, and V. A. Apkarian, "Visualizing vibrational normal modes of a single molecule with atomically confined light," Nature **568**, 78–82 (2019).
[9]B. Pettinger, B. Ren, G. Picardi, R. Schuster, and G. Ertl, "Nanoscale probing of adsorbed species by tip-enhanced Raman spectroscopy," Phys. Rev. Lett. **92**, 096101 (2004).
[10]E. Bailo and V. Deckert, "Tip-enhanced Raman scattering," Chem. Soc. Rev. **37**, 921–930 (2008).
[11]R. Zhang, Y. Zhang, Z. C. Dong, S. Jiang, C. Zhang, L. G. Chen, L. Zhang, Y. Liao, J. Aizpurua, Y. Luo, J. L. Yang, and J. G. Hou, "Chemical mapping of a single molecule by plasmon-enhanced Raman scattering," Nature **498**, 82–86 (2013).
[12]D. V. Chulhai, Z. Hu, J. E. Moore, X. Chen, and L. Jensen, "Theory of linear and nonlinear surface-enhanced vibrational spectroscopies," Ann. Rev. Phys. Chem. **67**, 541–564 (2016).
[13]S. M. Morton, D. W. Silverstein, and L. Jensen, "Theoretical studies of plasmonics using electronic structure methods," Chem. Rev. **111**, 3962–3994 (2011).
[14]L. Jensen, C. M. Aikens, and G. C. Schatz, "Electronic structure methods for studying surface-enhanced Raman scattering," Chem. Soc. Rev. **37**, 1061–1073 (2008).
[15]A. T. Zayak, Y. S. Hu, H. Choo, J. Bokor, S. Cabrini, P. J. Schuck, and J. B. Neaton, "Chemical Raman enhancement of organic adsorbates on metal surfaces," Phys. Rev. Lett. **106**, 083003 (2011).
[16]J. R. Lombardi and R. L. Birke, "A unified view of surface-enhanced Raman scattering," Acc. Chem. Res. **42**, 734–742 (2009).
[17]L. Zhao, L. Jensen, and G. C. Schatz, "Pyridine-Ag_{20} cluster: A model system for studying surface-enhanced Raman scattering," J. Am. Chem. Soc. **128**, 2911–2919 (2006).
[18]J. R. Lombardi and R. L. Birke, "A unified approach to surface-enhanced Raman spectroscopy," J. Phys. Chem. C **112**, 5605–5617 (2008).
[19]S. M. Morton and L. Jensen, "Understanding the molecule-surface chemical coupling in SERS," J. Am. Chem. Soc. **131**, 4090–4098 (2009).
[20]N. Valley, N. Greeneltch, R. P. Van Duyne, and G. C. Schatz, "A look at the origin and magnitude of the chemical contribution to the enhancement mechanism of surface-enhanced Raman spectroscopy (SERS): Theory and experiment," J. Phys. Chem. Lett. **4**, 2599–2604 (2013).
[21]A. K. Kuhlman and A. T. Zayak, "Revealing interaction of organic adsorbates with semiconductor surfaces using chemically enhanced Raman," J. Phys. Chem. Lett. **5**, 964–968 (2014).
[22]A. T. Zayak, H. Choo, Y. S. Hu, D. J. Gargas, S. Cabrini, J. Bokor, P. J. Schuck, and J. B. Neaton, "Harnessing chemical Raman enhancement for understanding organic adsorbate binding on metal surfaces," J. Phys. Chem. Lett. **3**, 1357–1362 (2012).
[23]F. L. Hirshfeld, "Bonded-atom fragments for describing molecular charge densities," Theor. Chim. Acta **44**, 129–138 (1977).
[24]L. Gagliardi, R. Lindh, and G. Karlström, "Local properties of quantum chemical systems: The LoProp approach," J. Chem. Phys. **121**, 4494–4500 (2004).
[25]B. Cordero, V. Gómez, A. E. Platero-Prats, M. Revés, J. Echeverría, E. Cremades, F. Barragán, and S. Alvarez, "Covalent radii revisited," Dalton Trans. **2008**, 2832–2838.
[26]E. J. Baerends, T. Ziegler, A. J. Atkins, J. Autschbach, D. Bashford, O. Baseggio, A. Bérces, F. M. Bickelhaupt, C. Bo, P. M. Boerritger, L. Cavallo, C. Daul, D. P. Chong, D. V. Chulhai, L. Deng, R. M. Dickson, J. M. Dieterich, D. E. Ellis, M. van Faassen, A. Ghysels, A. Giammona, S. J. A. van Gisbergen, A. Goez, A. W. Götz, S. Gusarov, F. E. Harris, P. van den Hoek, Z. Hu, C. R. Jacob, H. Jacobsen, L. Jensen, L. Joubert, J. W. Kaminski, G. van Kessel, C. König, F. Kootstra, A. Kovalenko, M. Krykunov, E. van Lenthe, D. A. McCormack, A. Michalak, M. Mitoraj, S. M. Morton, J. Neugebauer, V. P. Nicu, L. Noodleman, V. P. Osinga, S. Patchkovskii, M. Pavanello, C. A. Peeples, P. H. T. Philipsen, D. Post, C. C. Pye, H. Ramanantoanina, P. Ramos, W. Ravenek, J. I. Rodríguez, P. Ros, R. Rüger, P. R. T. Schipper, D. Schlüns, H. van Schoot, G. Schreckenbach, J. S. Seldenthuis, M. Seth, J. G. Snijders, M. Solà, M. Solà, M. Swart, D. Swerhone, G. te Velde, V. Tognetti, P. Vernooijs, L. Versluis, L. Visscher, O. Visser, F. Wang, T. A. Wesolowski, E. M. van Wezenbeek, G. Wiesenekker, S. K. Wolff, T. K. Woo, and A. L. Yakovlev, ADF2018, SCM, Theoretical Chemistry, Vrije Universiteit, Amsterdam, The Netherlands, https://www.scm.com, 2018.
[27]G. te Velde, F. M. Bickelhaupt, E. J. Baerends, C. Fonseca Guerra, S. J. A. van Gisbergen, J. G. Snijders, and T. Ziegler, "Chemistry with ADF," J. Comput. Chem. **22**, 931–967 (2001).
[28]A. D. Becke, "Density-functional exchange-energy approximation with correct asymtotic-behavior," Phys. Rev. A **38**, 3098–3100 (1988).
[29]J. P. Perdew, "Density-functional approximation for the correlation energy of the inhomogeneous electron gas," Phys. Rev. B **33**, 8822–8824 (1986).
[30]E. van Lenthe, E. J. Baerends, and J. G. Snijders, "Relativistic regular two-component Hamiltonians," J. Chem. Phys. **99**, 4597–4610 (1993).
[31]L. Jensen, J. Autschbach, and G. C. Schatz, "Finite lifetime effects on the polarizability within time-dependent density-functional theory," J. Chem. Phys. **122**, 224115 (2005).
[32]L. Jensen, L. L. Zhao, J. Autschbach, and G. C. Schatz, "Theory and method for calculating resonance Raman scattering from resonance polarizability derivatives," J. Chem. Phys. **123**, 174110 (2005).
[33]The PyMOL molecular graphics system, version 1.2r3pre, Schrödinger, LLC, 2019.
[34]P. Johansson, "Illustrative direct *ab initio* calculations of surface Raman spectra," Phys. Chem. Chem. Phys. **7**, 475–482 (2005).
[35]J. E. Moore, S. M. Morton, and L. Jensen, "Importance of correctly describing charge-transfer excitations for understanding the chemical effect in SERS," J. Phys. Chem. Lett. **3**, 2470–2475 (2012).
[36]J. F. DeJesus, M. J. Trujillo, J. P. Camden, and D. M. Jenkins, "*N*-heterocyclic carbenes as a robust platform for surface-enhanced Raman spectroscopy," J. Am. Chem. Soc. **140**, 1247–1250 (2018).
[37]M. J. Trujillo, J. C. Becca, S. L. Strausser *et al.*, "Using SERS to understand the binding of *N*-heterocyclic carbenes to gold surfaces," J. Phys. Chem. Lett. **9**, 6779–6785 (2018).
[38]C. F. Guerra, J.-W. Handgraaf, E. J. Baerends, and F. M. Bickelhaupt, "Voronoi deformation density (VDD) charges: Assessment of the Mulliken, Bader, Hirshfeld, Weinhold, and VDD methods for charge analysis," J. Comput. Chem. **25**, 189–210 (2004).
[39]K. B. Wiberg and P. R. Rablen, "Comparison of atomic charges derived via different procedures," J. Comput. Chem. **14**, 1504–1518 (1993).
[40]P. Bultinck, C. V. Alsenoy, P. W. Ayers, and R. Carbó-Dorca, "Critical analysis and extension of the Hirshfeld atoms in molecules," J. Chem. Phys. **126**, 144111 (2007).
[41]P. Verma, "Tip-enhanced Raman spectroscopy: Technique and recent advances," Chem. Rev. **117**, 6447–6466 (2017).
[42]S. Zaleski, A. J. Wilson, M. Mattei, X. Chen, G. Goubert, M. F. Cardinal, K. A. Willets, and R. P. Van Duyne, "Investigating nanoscale electrochemistry with surface- and tip-enhanced Raman spectroscopy," Acc. Chem. Res. **49**, 2023–2030 (2016).
[43]H. Song, M. A. Reed, and T. Lee, "Single molecule electronic devices," Adv. Mater. **23**, 1583–1608 (2011).

Published under license by AIP Publishing